A Novel Strategy for Three-phase/switch/level (Vienna) Rectifier under Severe Unbalanced Grids

Ming Zhang, Bin Li, Long Huang,
Wenxi Yao, Zhengyu Lu
College of Electrical Engineering, Zhejiang University
National Laboratory of Power Electronics
Hangzhou, Zhejiang Province, China
eezmzju@gmail.com

Lijun Hang, Leon M. Tolbert
Department of Electrical Engineering and Computer Science
The University of Tennessee
Knoxville, TN 37996-2250 USA
leejean.hang@gmail.com
tolbert@utk.edu

***Abstract*—Unbalanced grids introduce performance deterioration for the Vienna rectifier topology by producing twice fundamental frequency ripple in the dc-link voltage and input active/reactive power. A traditional control strategy is the input current tracking scheme, which can work under any unbalanced conditions, but it cannot eliminate the input power ripple and the output dc-link voltage ripple. Another class of control strategy for the purpose of eliminating the input power ripple can maintain constant input power and eliminate the dc-link voltage ripple, however, it will fail under severe unbalanced grids. This paper first analyzes the theoretical limits of constant power control method, and based on which a novel control method that injects a small amount of power ripple is proposed to make a compromise between the working area and the output dc voltage ripple. Finally, the experiment results using constant power control method are given and validate the performance of the proposed control method.**

I. INTRODUCTION

The unidirectional three-phase/switch/level Vienna rectifier has the merits of low cost, high power density, high reliability, and lower EMI. It is used in the applications of aircraft power supplies, medium voltage drives, telecommunication and active filters where power density and voltage stress are of utmost importance. For non-regenerative Vienna-type rectifiers, the rectifier input phase voltage is influenced not only by the switching states, but also by the direction of the associated mains phase current [1-4]. For its unidirectional power flow characteristic, it will introduce second harmonic ripple in the dc-link side and low order odd harmonics in the ac side under unbalanced grids.

According to the symmetrical component method, unbalanced grid voltage can be divided into positive, negative and zero sequence symmetrical voltage components. The component of zero sequence has no effect in three-wire systems and can be ignored. A traditional control strategy is to make the input phase current track the input differential voltage component, which maintains the synchronization of the input current vector and the input voltage vector. This control strategy can work under any unbalanced conditions, and is easy to implement, but it cannot eliminate the input power ripple and output dc-link voltage ripple [5][6]. Another control strategy is based on the active and reactive power equations, such as dual-frame hybrid vector control (DFHVC), which directly generates the positive and negative sequence current reference to eliminate the input power ripple and maintain the input power as constant value [7][8][9]. However, it can only work under light unbalanced utility grids and would fail when under severe unbalanced condition because there is large angle difference between the input current and input voltage vector. Furthermore, the critical working area has not been explained yet.

In this paper, the theoretical operation area of applying constant power control strategy is analyzed first, and then a novel control method by injecting a small amount of power ripple is proposed in the third section. A simplified control algorithm realized in abc stationary coordinates is proposed in the fourth section, and the experimental comparison results of the above three types of control strategies, including current tracking, constant power control and the proposed method are given in the fifth section. Finally, the conclusion remarks are given in the final section.

II. OPERATION AREA OF CONSTANT POWER CONTROL STRATEGY UNDER UNBALANCED GRIDS

The topology of the three-phase/switch/level Vienna unidirectional rectifier is shown in Fig. 1, which consists of 18 diodes and 3 MOSFETs crossing over the input inductor and the output neutral point of *M*. The rectifier input

This work was supported by the National Natural Science Foundation of China (51177148) and Zhejiang Key Science and Technology Innovation Group Program (2010R50021).

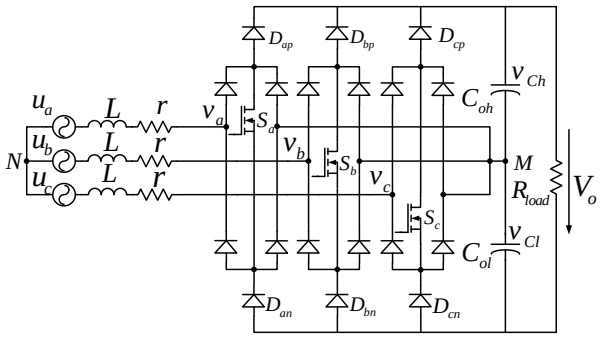

Fig. 1. Three-phase/switch/level unidirectional Vienna rectifier.

voltage (v_{am}, v_{bm}, v_{cm}) is determined by the corresponding switch state and the polarity of the input current, so v_{am}, v_{bm} and v_{cm} can get three levels as $\{+V_o/2, 0, -V_o/2\}$, where V_o is the output dc voltage as shown in Fig. 1. According to the different combinations of input voltage levels, 25 different voltage vectors can be achieved in α-β plane as shown in Fig. 2.

The relationship of possible vectors, corresponding switches states, and the dc-link voltage is analyzed in detail in [11]. Here, the explanation is summarized. The rectifier input voltage level is determined by the polarity of input current and the switch state, and only 2 levels could be realized at the same time. For example, assuming i_a>0, if S_a is ON, v_{aM} is zero, and if S_a is OFF, then v_{aM} is $+V_o/2$, so only $\{+V_o/2, 0\}$ can be achieved at this time. Therefore, Vienna rectifier topology can realize only eight voltage vectors at any given time. These realizable voltage vectors are determined by the region the input current vector $i_{\alpha\beta}$ located. So the input current vector $i_{\alpha\beta}$ divides the whole α-β plane into six regions shown in Fig. 2 (Region I, II, III, IV, V, VI) for the convenience of vector analysis. Taking region I as an example, the voltage vectors that can be achieved are located in the shaded hexagon, including six vectors at six vertices and two redundant vectors at the hexagon center. In this region, by the constraint of three-phase current polarity, only one state of the upper and lower redundant vectors can be achieved, they are state [0 -1 0] for the lower one and state [0 0 -1] for the upper one.

Based on the above analysis, when the input current vector situates in region I, if the rectifier input voltage vector exceeds the shaded hexagon area, the rectifier will fail to work. In α-β plane, the Vienna rectifier voltage equation can be written as:

$$u_{\alpha\beta} = r \cdot i_{\alpha\beta} + j\omega L \cdot i_{\alpha\beta} + v_{\alpha\beta} \quad (1)$$

where, $u_{\alpha\beta}, i_{\alpha\beta}$ and$v_{\alpha\beta}$are the grid voltage vector, the input current vector and the rectifier input voltage vector respectively, r and L are the equivalent resistance and inductance of input inductor respectively. ω is the grid angular frequency. If the voltage across the input inductor is ignored, the grid voltage vector will be equal with the rectifier input voltage vector. As shown in Fig. 3, when the input current vector reaches the boundary AE, the corresponding voltage vector should be above line AF and FE.

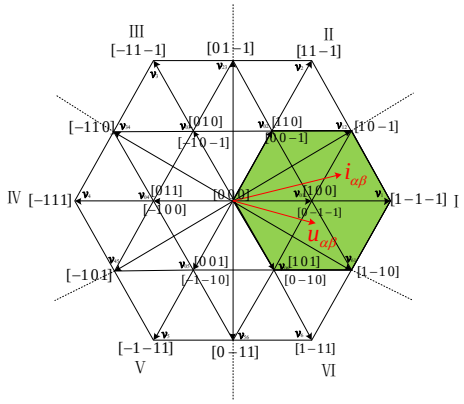

Fig. 2. 25-voltage vectors for Vienna rectifier in α-β plane.

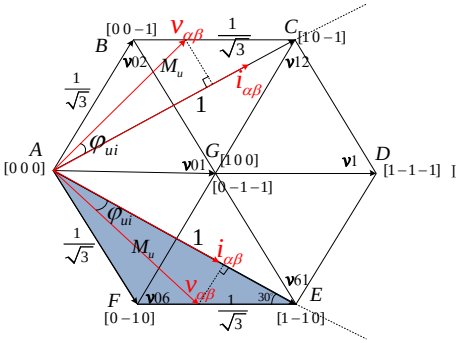

Fig. 3. 8-voltage vectors that could be achieved when the input current is situated in region I.

When the phase angle lags between the input voltage vector and the input current vector is too large, the input voltage vector will separate from the shaded hexagon area shown in Fig. 2, and then Vienna rectifier will fail to work. By ignoring the voltage drop across the input inductor, the situation is the same when the current vector locates at the upper boundary AC as at the low boundary AE.

Assuming $M_u = |v_{\alpha\beta}|/|v_{61}|$, and the middle voltage vector length $V_o/\sqrt{3}$ is normalized as a unit length. From the geometric relationships shown in Fig. 3, we can obtain the required condition which should be fulfilled for the Vienna rectifier as follows:

$$|\varphi_{ui}| \le \min\left(\arcsin\left(\frac{1}{2M_u}\right) - \frac{\pi}{6}, \frac{\pi}{6}\right) \quad (2)$$

where, φ_{ui} is shown in Fig. 3. When M_u is larger than $1/\sqrt{3}$, $|\varphi_{ui}|$ should be less than the former value in (2), otherwise $|\varphi_{ui}|$ should be less than $\pi/6$.

The three unbalanced voltages can be described as (3), here the non-functioning zero sequence is ignored.

$$\begin{pmatrix} v_a \\ v_b \\ v_c \end{pmatrix} = A_p \cdot \begin{pmatrix} \sin(\omega t) \\ \sin\left(\omega t - \frac{2\pi}{3}\right) \\ \sin\left(\omega t + \frac{2\pi}{3}\right) \end{pmatrix} + A_n \cdot \begin{pmatrix} \sin(\omega t + \varphi) \\ \sin\left(\omega t + \frac{2\pi}{3} + \varphi\right) \\ \sin\left(\omega t - \frac{2\pi}{3} + \varphi\right) \end{pmatrix} \quad (3)$$

A_p and A_n are the amplitude of the positive and negative voltage sequence.

The active and reactive power equation on d-q axis is shown in (4) (see [7] for details,):

$$\begin{pmatrix} V_{dp} & V_{qp} & V_{dn} & V_{qn} \\ V_{qn} & -V_{dn} & -V_{qp} & V_{dp} \\ V_{qp} & -V_{dp} & -V_{qn} & V_{dn} \\ V_{dn} & V_{qn} & V_{dp} & V_{qp} \end{pmatrix} \cdot \begin{pmatrix} I_{dp} \\ I_{qp} \\ I_{dn} \\ I_{qn} \end{pmatrix} = \begin{pmatrix} P \\ P_{s2} \\ Q \\ P_{c2} \end{pmatrix} \quad (4)$$

P and Q are active and reactive power, P_{s2}, P_{c2} are the amplitude of second order power ripple. Set P_{s2}, P_{c2}, Q in (4) to be zero, then the current reference by applying constant power control strategy could be obtained, and meanwhile apply positive and negative synchronous rotation coordinate transformation to the current reference, we can get the three-phase current reference in abc-stationary frame as (5):

$$\begin{pmatrix} i_a \\ i_b \\ i_c \end{pmatrix} = \frac{P}{1.5(A_p^2 - A_n^2)} \cdot \begin{pmatrix} v_{ap} - v_{an} \\ v_{bp} - v_{bn} \\ v_{cp} - v_{cn} \end{pmatrix} \quad (5)$$

Define $\gamma = A_n/A_p$ as the grid voltage unbalanced factor and select A_p as the voltage base value, $2PA_p/[3(A_p^2-A_n^2)]$ as the current base value, then the voltage vector and current vector reference can be normalized. Rewrite the normalized results in α-β plane as (6) and (7).

$$\begin{pmatrix} v_\alpha \\ v_\beta \end{pmatrix} = \begin{pmatrix} \sin(\omega t) \\ -\cos(\omega t) \end{pmatrix} + \gamma \cdot \begin{pmatrix} \sin(\omega t + \varphi) \\ \cos(\omega t + \varphi) \end{pmatrix} \quad (6)$$

$$\begin{pmatrix} i_\alpha \\ i_\beta \end{pmatrix} = \begin{pmatrix} \sin(\omega t) \\ -\cos(\omega t) \end{pmatrix} - \gamma \cdot \begin{pmatrix} \sin(\omega t + \varphi) \\ \cos(\omega t + \varphi) \end{pmatrix} \quad (7)$$

Applying a rotating transformation as (8) which makes a clockwise rotation to α-β frame by $\varphi/2$, namely $\alpha'\beta'$ plane as shown in Fig. 4. In $\alpha'\beta'$ plane, the voltage and current reference vector can be written as (9).

$$\begin{pmatrix} x'_\alpha \\ x'_\beta \end{pmatrix} = \begin{pmatrix} \cos(\varphi/2) & -\sin(\varphi/2) \\ \sin(\varphi/2) & \cos(\varphi/2) \end{pmatrix} \cdot \begin{pmatrix} x_\alpha \\ x_\beta \end{pmatrix} \quad (8)$$

$$\begin{pmatrix} v'_\alpha \\ v'_\beta \end{pmatrix} = \begin{pmatrix} (1+\gamma) \cdot \cos\theta \\ (1-\gamma) \cdot \sin\theta \end{pmatrix}, \begin{pmatrix} i'_\alpha \\ i'_\beta \end{pmatrix} = \begin{pmatrix} (1-\gamma) \cdot \cos\theta \\ (1+\gamma) \cdot \sin\theta \end{pmatrix} \quad (9)$$

As shown in Fig. 4, the angle of boundary axis of six regions clockwise is rotated by $\varphi/2$ to $\alpha'\beta'$ plane, which is shown in (10). According to (9) and Fig. 5, the angle between the voltage and current vector and the amplitude of the voltage vector can be easily derived, which is shown in (11). The current vector's phase angle Φ_i is shown in Fig. 5.

The results in (11) are based on normalized values, and K is the normalized amplitude of the voltage vector with its base value of $M_0 = \sqrt{3}A_p/V_o$. Based on (2) and (11), the theoretical operation area of the Vienna topology under unbalanced grids is given in (12).

$$\begin{cases} axis-A: \frac{\pi}{2}(\alpha\beta) \rightarrow \frac{\pi}{2} + \frac{\varphi}{2}(\alpha'\beta') \\ axis-B: \frac{\pi}{6}(\alpha\beta) \rightarrow \frac{\pi}{6} + \frac{\varphi}{2}(\alpha'\beta') \\ axis-C: -\frac{\pi}{6}(\alpha\beta) \rightarrow -\frac{\pi}{6} + \frac{\varphi}{2}(\alpha'\beta') \end{cases} \quad (10)$$

The parameters in (11) and (12) can be found in the previous analysis. From (11) and (12), we can see that the

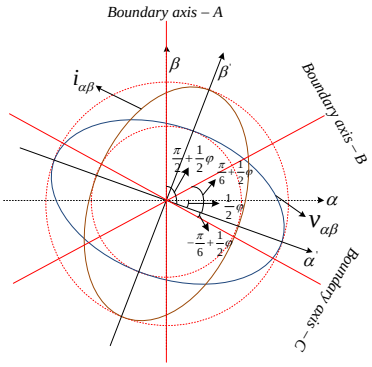

Fig. 4. The input voltage vector and current vector locus in α-β and α'-β' plane.

$$\begin{cases} \varphi_{ui} = \arctan\left(\frac{(1-\beta)\tan(\Phi_i)}{1+\beta^2 tan^2(\Phi_i)}\right) \\ K = \sqrt{\frac{1+\beta^2 tan^2(\Phi_i)}{1+\beta tan^2(\Phi_i)}}(1+\gamma) \\ \beta = \left(\frac{1-\gamma}{1+\gamma}\right)^2 \end{cases} \quad (11)$$

$$\begin{cases} |\varphi_{ui}| \le \min(\arcsin\left(\frac{1}{2M_u}\right) - \frac{\pi}{6}, \frac{\pi}{6}) \\ M_u = M_0 \cdot K = \frac{\sqrt{3}A_p}{V_o} \cdot \sqrt{\frac{1+\beta^2 tan^2(\Phi_i)}{1+\beta tan^2(\Phi_i)}}(1+\gamma) \end{cases} \quad (12)$$

operation area is related with the grid voltage unbalanced factor γ, the positive sequence modulation index M_0 and the phase difference φ of positive and negative sequence voltage. Considering that the input current vector has six boundary axes (because the input current vector crosses over all six regions) in a line frequency cycle, so only $\varphi \in \{0, \pi/3\}$ need to be considered. When $\varphi = \pi/6$ or nearby,

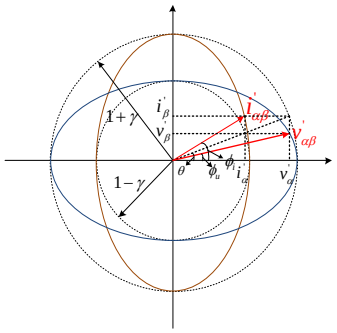

Fig. 5. Analysis of the input voltage and current vector in α'-β' plane.

the rectifier has a relatively larger working area, but the difference is very small. The working area is mainly decided by the positive sequence modulation index M_0 and the grid voltage unbalance factor γ. Fig. 10 gives the relationship between the above two factors in section V.

III. Control Method under Different Unbalanced Grids

In order to expand the operating area of the constant power control strategy under severe unbalanced grids, the angle

between the input voltage and current vector reference must be decreased. For an intuitive statement, the voltage and current vector locus are drawn in a positive synchronous rotation frame in Fig. 6. For the purpose of reducing the angle of the voltage and current vector, an additional current vector is added to the current vector reference as shown in Fig. 6 and (13):

$$i_{dq} = i_{dq}^{0} + f \cdot i'_{dq} \tag{13}$$

i_{dq}^{0} is the original current vector, $f \cdot i'_{dq}$ is the additional current vector, and f represents the input power ripple injection rate and it is decided by the grid voltage unbalance factor and the positive sequence modulation index. These two vectors in Fig. 6 can be normalized as the following description:

$$\begin{cases} i_{dq}^{0} = (V_{dp} \;\; V_{qp} \;\; -V_{dn} \;\; -V_{qn})^{T} \\ i'_{dq} = (0 \;\;\; 0 \;\;\; V_{dn} \;\;\; V_{qn})^{T} \end{cases} \tag{14}$$

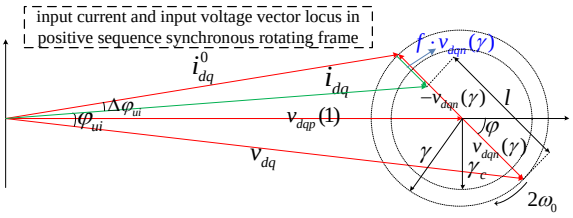

Fig. 6. The input voltage and current vector locus in positive synchronous rotation frame.

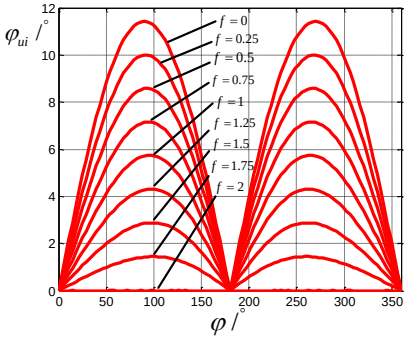

Remarks: x-axis label: phase difference of the negative and positive component in the positive sequence synchronous rotating frame in a half line cycle, as shown in Fig. 6. (angle speed of negative sequence is twice of line frequency.)

y-axis label: phase difference of the voltage and current vector in a half line cycle.

Fig. 7. The angle of the voltage and current vector under different value of f in a half line cycle period (γ=0.1).

Applying (14) into (13), the new current reference vector can be obtained, and can be rewritten into abc-stationary frame as follows,

$$\begin{cases} i_a = v_{ap} + (-1+f) \cdot v_{an} \\ i_b = v_{bp} + (-1+f) \cdot v_{bn} \\ i_c = v_{cp} + (-1+f) \cdot v_{cn} \end{cases} \tag{15}$$

Equation (15) is based on the normalized values, applying

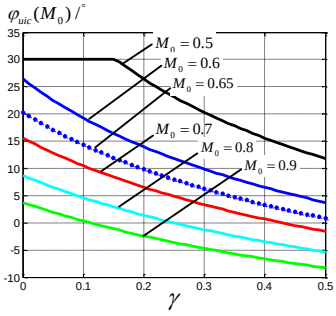

Fig. 8. The critical angle $\varphi_{uic}(M_0)$ of the voltage and current vector (decided by (2)) curves as the grid voltage unbalanced factor varies in the maximum voltage vector length case under different positive voltage sequence modulation index.

$$\begin{pmatrix} i_a \\ i_b \\ i_c \end{pmatrix} = \frac{P}{1.5(A_p^2 + (-1+f) \cdot A_n^2)} \cdot \begin{pmatrix} v_{ap} + (-1+f) \cdot v_{an} \\ v_{bp} + (-1+f) \cdot v_{bn} \\ v_{cp} + (-1+f) \cdot v_{cn} \end{pmatrix} \tag{16}$$

the instantaneous power balance equation into (15), the real value of the current reference is easy to be obtained as (16).

The power ripple injection rate is represented by the value of f, when f=0, no power ripple is injected and this is equal to the constant power control method. When f=2, the injected power ripple is maximum and this is equal to the current tracking scheme. While in this work, $0 < f < 2$ is chosen to achieve the balance between the output dc-link voltage ripple and operation area.

Based on the above analysis, when the input voltage unbalance factor exceeds the critical value $\gamma_c(M_0)$, which is defined as the critical unbalance factor of the constant power control strategy analyzed above under a certain positive sequence voltage modulation index M_0, then by controlling f>0, an input power ripple is injected to decrease the angle between voltage vector and current vector reference, then the Vienna rectifier will be able to work properly.

$\varphi_{uic}(M_0)$ is defined as the maximum allowable angle between the voltage vector and current vector before Vienna rectifier fails. The increase of the negative sequence voltage component will cause two effects. First, the angle of the voltage and current vector becomes larger than before, which is clearly shown in Fig. 6, and second, as the negative sequence increases, the critical angle $\varphi_{uic}(M_0)$ becomes smaller than before, which can be derived from (2). In order to eliminate these two effects, the parameter f is decomposed into two parts, i.e. f_1 and f_2, to compensate them respectively.

First, the angle of the voltage and current vector should be calculated. It can be expressed by the length of the voltage vector endpoint and current vector endpoint as *"l"*, which is shown in Fig. 6. Fig. 7 gives the angle under different f and shows the correctness of this approximation. Then the critical angle $\varphi_{uic}(M_0)$ can be represented by the length of $2\gamma_c$.

For the first effect as mentioned above, in order to keep the angle the same as the original critical angle $\varphi_{uic}(M_0)$, here we assume that the second effect is ignored, so f_1 will just

need to change the length l into the critical length $2\gamma_c$, as shown in Fig. 6, we have:

$$f_1 \cdot \gamma = 2\gamma - 2\gamma_c \tag{17}$$

And for the second effect, as the length of voltage vector increases, the critical angle $\varphi_{uic}(M_0)$ will be reduced. Take the worst case as an example, when $|v_{\alpha\beta}| = M_0(1+\gamma)$, the critical angle decided by (2) is approximated linearly as shown in Fig. 8, and the parameter k_φ is used to measure the change of the critical angle as the length of voltage vector varies. k_φ is the constant of about 2/3, which could be derived from Fig. 8. From this point of view, and based on the angle-length approximation, the other part of f, namely f_2 should meet the following qualification.

$$f_2 \cdot 2\gamma_c = k_\varphi \cdot (\gamma - \gamma_c) \tag{18}$$

Combine (17) and (18), the parameter f is defined as:

$$f = \begin{cases} 0 & (\gamma < \gamma_c) \\ \min\left\{\frac{4}{3} + \frac{4}{3}\cdot\frac{\gamma}{\gamma_c} - 2\cdot\frac{\gamma_c}{\gamma}, 2\right\} & (\gamma > \gamma_c) \end{cases} \tag{19}$$

$\gamma_c(M_0)$ is about 90% of the range of experimental verification area, its approximate fitting function with the positive voltage sequence modulation index is shown in (20).

$$\gamma_c(M_0) = \min(0.42 \cdot M_0^2 - 0.98 \cdot M_0 + 0.548, 0.18) \tag{20}$$

According to (16), (19) and (20), the new current reference can be calculated.

IV. Control System Design

Based on the above analysis, the new current reference on abc-stationary frame is obtained, so the complex rotating coordinate transformation and phase-locked loop is avoided, which greatly simplifies the control system architecture and algorithms. And the only work is to extract the positive and negative components from the original three-phase voltages.

A novel filter algorithm to extract the positive and negative components in α-β frame is proposed in [10], and is adopted in this paper. Equation (21) shows a one-order high-pass filter in positive sequence synchronous rotating frame,

$$H_{dq}(s) = \frac{s}{s+\omega_c} \tag{21}$$

Equation (21) is equal to (22) in α-β plane, as, (see [10] for details,)

$$H_{\alpha\beta}(s) = \begin{pmatrix} \frac{s^2+\omega_c s+\omega^2}{s^2+2\omega_c s+\omega_c^2+\omega^2} & \frac{-\omega\omega_c}{s^2+2\omega_c s+\omega_c^2+\omega^2} \\ \frac{\omega\omega_c}{s^2+2\omega_c s+\omega_c^2+\omega^2} & \frac{s^2+\omega_c s+\omega^2}{s^2+2\omega_c s+\omega_c^2+\omega^2} \end{pmatrix} \tag{22}$$

Then the extraction process can be described as the following expression, and the transformation matrixes are defined as (24) and (25) respectively.

$$\begin{pmatrix} v_{an} \\ v_{bn} \end{pmatrix} = \boldsymbol{T_{\alpha\beta\to abc}} \cdot H_{\alpha\beta}(s) \cdot \boldsymbol{T_{abc\to\alpha\beta}} \cdot \begin{pmatrix} v_a \\ v_b \end{pmatrix} \tag{23}$$

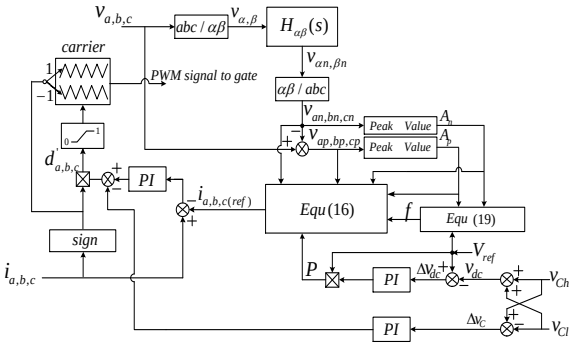

Fig. 9. The whole control system of the proposed control method of three-phase/switch/level Vienna-type rectifier under unbalanced grids.

$$\boldsymbol{T_{\alpha\beta\to abc}} = \begin{pmatrix} 0 & 1 \\ \sqrt{3}/2 & -1/2 \end{pmatrix} \tag{24}$$

$$\boldsymbol{T_{abc\to\alpha\beta}} = \begin{pmatrix} 1/\sqrt{3} & 2/\sqrt{3} \\ 1 & 0 \end{pmatrix} \tag{25}$$

In the above equations, v_a, v_b and v_c are the three phase input voltages. The above decoupling method avoids the complex calculations in d-q axis and it is easy to implement. The whole control system architecture is shown in Fig. 9. The dc voltage loop and the current loop were designed by selecting their corresponding bandwidth. Here, $\omega_c = 25rad/s$ is selected in (21).

V. Experiments and Results

Table I gives the balanced grid and prototype parameters. The programmable ac source is used to emulate the three-phase grid. The whole controller is implemented in a floating point microcontroller unit TMS320F28335 from TI. The prototype of Vienna converter was built in the laboratory based on discrete MOSFETs and diodes.

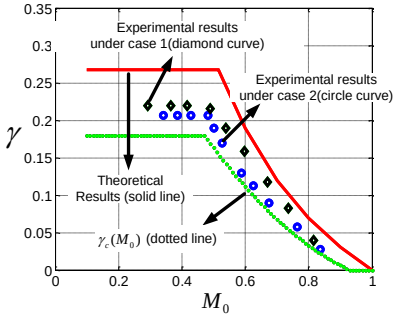

Remarks: Case 1 (diamond curve): phase difference of phase-A and phase-B is only changed; Case 2 (circle curve): phase-A input voltage is only changed; The solid curve is the theory operation area, calculated by (2); The dotted curve is the critical grid voltage unbalanced factor ($\gamma_c(M_0)$, in (20)) in the prototype.

Fig. 10. Experimental operation area of constant power control strategy.

As shown in Table I, the rating output voltage is 240 V and the rating load is 70 Ohm. The rating input voltage is 50 V_{ac} at 50 Hz. The rated output power is 822 W at balanced load condition. The unbalanced condition described in this implementation is based on the above balanced condition.

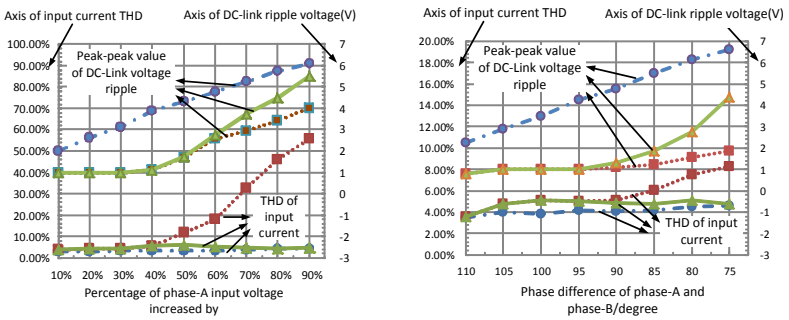

(a) (b)

Remarks: Type1 (circle curve):input current traces input voltage; Type2 (square curve): constant power control; Type3 (triangle curve):proposed compromise control method.

Fig. 11. (a)Performance comparison between three types control strategies under voltage unbalanced conditions; (b)Performance comparison between three types control strategies under phase unbalanced conditions.

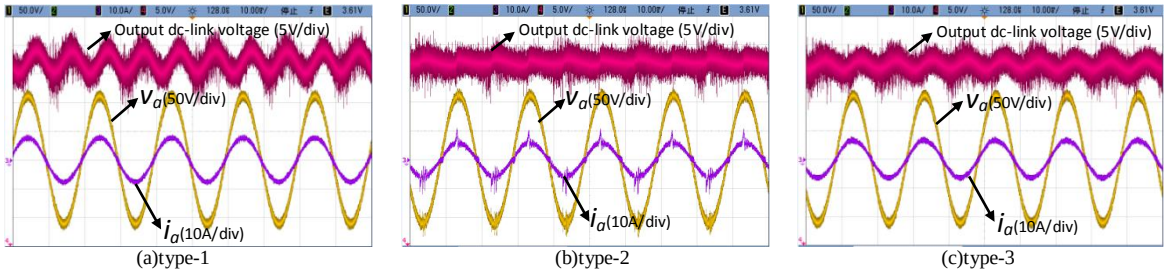

(a)type-1 (b)type-2 (c)type-3

Fig. 12. Performance of three types control strategies under the condition: phase-A input voltage increases by 60%.

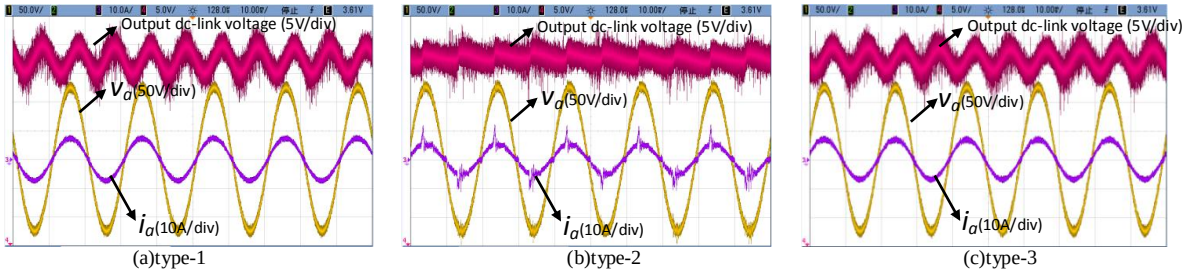

(a)type-1 (b)type-2 (c)type-3

Fig. 13. Performance of three types control strategies under the condition: phase-A input voltage increases by 80%.

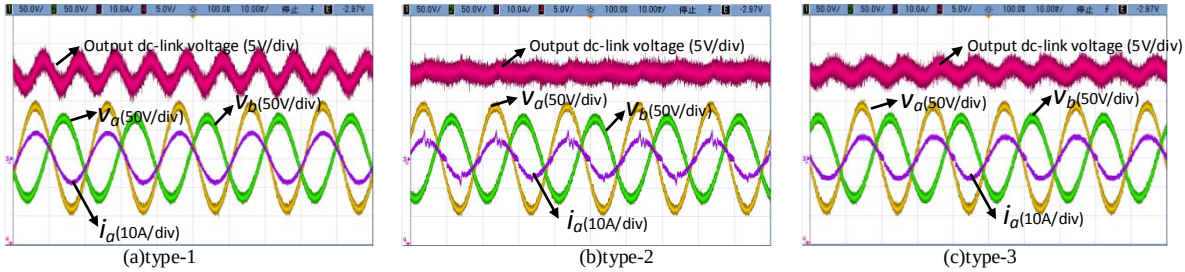

(a)type-1 (b)type-2 (c)type-3

Fig. 14. Performance of three types control strategies under the condition: phase-A input voltage increases by 30%, and phase difference of phase-A and phase-B voltage is 140 degree.

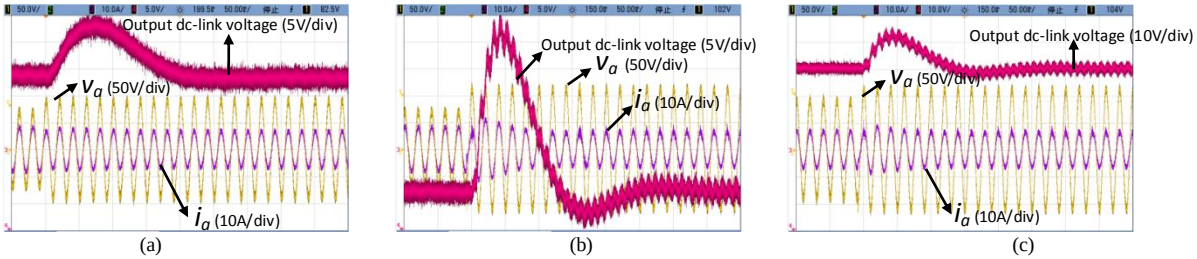

(a) (b) (c)

Fig. 15. Waveforms with proposed control method when the phase-A input voltage has a mutation. Define: 1):Light unbalanced grid: phase-A input voltage increases by 30%; 2):severe unbalanced grid: phase-A input voltage increases by 60%. (a) balanced grid changes into a light unbalanced grid; (b) balanced grid changes into a severe unbalanced grid; (c) light unbalanced grid changes into a severe unbalanced grid.

TABLE I. BALANCED GRID AND PROTOTYPE PARAMETERS

Three-phase voltage	50 Vrms
Output dc-link voltage	240 V_{dc}
Input inductance	360 uH
Output capacitance	2820 uF
Load resistance	70 Ohm
Switching frequency	50 kHz

The operation area of constant power control strategy is tested in two aspects: 1) only the amplitude of phase-A input voltage is changed; 2) only the phase difference between phase-A and phase-B is changed. Under these two conditions, the working area of the constant power control strategy is shown in Fig. 10.

Considering the circuit delay and bandwidth response of the inner current loop, the actual working area of constant power control strategy is smaller than that given by the theory analysis. However, the simulation results reveal that with the increase of current loop bandwidth, the working area will gradually approach the theoretical analysis as the solid curve shown in Fig. 10.

Fig. 11(a) and Fig. 11(b) give the performance of three control strategies under different unbalanced grids. Voltage unbalanced condition is given in Fig. 11(a), and phase unbalanced condition is given in Fig. 11(b). From the results of Fig. 11(a) and Fig. 11(b), the proposed control method has the performance between type-1 and type-2. Compared with type-2 (constant power control), the proposed control (type-3) has a more wide working area, and as to type-1(the input current tracking strategy), it has less input power ripple and output dc-link voltage ripple.

Fig. 12 and Fig. 13 give the key waveforms under different amplitude unbalance for phase A at the grids with three types of control strategies. It can be seen that the current performance is much better using type-1 control than using type-2 control, however the output voltage ripple is much larger. From Fig. 12(c) and Fig. 13 (c), it can be concluded that a comprised performance between current quality and output voltage ripple for the converter can be achieved by using the proposed controller when phase A has 60% and 80% voltage increase. Fig. 14 gives the waveforms under the condition with voltage-unbalance and phase unbalance by using three types of control strategies. Similar results are achieved in Fig. 14(a), Fig. 14(b) and Fig. 14(c). Compared with Fig. 14(a) and Fig. 14(b), relative good current quality and small output voltage ripple are achieved by using the proposed controller. The dynamic performance of the proposed control method is shown in Fig. 15 under different degrees of unbalanced grid. It can be seen from Fig. 15 that the proposed control scheme has a very fast response on the grid unbalance, and could complete the separation of positive and negative sequence, and the injection of power ripple in less than a line frequency cycle, which ensures a low input current distortion.

The proposed control strategy has achieved the operation area expansion under unbalanced grids. It can eliminate the ripples of the input power and output dc-link voltage under light unbalanced conditions, while under severe unbalanced conditions it can reduce the ripple of the input power and dc-link voltage. In addition, it can adjust the control schemes based on the working environment, which is adaptable to different unbalanced grids.

VI. CONCLUSION

In this paper, the operation area of Vienna rectifier by applying constant power control strategy is first analyzed, and then a control method to extend the working area by injecting a small amount of power ripple is proposed. Finally, the proposed control method is implemented in abc-stationary frame, which has the advantage of simplicity of control structure and algorithm. The balance of working area and output dc-link voltage ripple is achieved. A prototype was built to verify the theoretical analysis and a series of experimental results are given in the paper.

REFERENCES

[1] J. W. Kolar and F. C. Zach, "A novel three-phase utility interface minimizing line current harmonics of high-power telecommunications rectifier modules," *IEEE Trans. Ind. Electron.*, vol. 44, no. 4, pp. 456-467, Aug. 1997.

[2] N. B. H. Youssef, K. Al-Haddad, and H. Y. Kanaan, "Large-signal modeling and steady-state analysis of a 1.5-kW three-phase/switch/level (Vienna) rectifier with experimental validation," *IEEE Trans. Ind. Electron.*, vol. 55, no. 3, pp. 1213-1224, March 2008.

[3] M. Zhang, B. Li, L. Hang, L. M Tolbert and Z. Lu, "Performance study for high power density three-phase Vienna PFC rectifier by using SVPWM control method," in *IEEE Proc. Appl. Power Electron. Conf. Expo.*, 2012, pp. 1187-1191.

[4] R. Lai, F. Wang, R. Burgos, D. Boroyevich, J. Dong, D. Zhang, "Average modeling and control design for VIENNA-type rectifiers considering the DC-link voltage balance," *IEEE Trans. Power Electron.*, vol. 24, no. 11, pp. 2509-2522, Nov. 2009.

[5] J. Minibock, and J. W. Kolar, "Novel concept for mains voltage proportional input current shaping of a VIENNA rectifier eliminating controller multipliers," *IEEE Trans. Ind. Electron.*, vol. 52, no. 1, pp. 162–170, Feb. 2005.

[6] P. Rioual, H. Pouliquen and J. Louis, "Regulation of a PWM rectifier in the unbalanced network state using a generalized model," *IEEE Trans. Power Electron.*, vol. 11, no. 3, pp. 495-502, May 1996.

[7] H. Teshnizi, A. Moallem, M. R. Zolghadri, and M. Ferdowsi, "A dual-frame hybrid vector control of vector modulated VIENNA I rectifier for unity power factor operation under unbalanced mains condition," in *IEEE Proc. Appl. Power Electron. Conf. Expo.*, 2008, pp. 1402-1408.

[8] Y. Bo, R. Oruganti, S. K. Panda, and A. K. S Bhat, "An output-power-control strategy for a three-phase PWM rectifier under unbalanced supply conditions," *IEEE Trans. Ind. Electron.*, vol. 55, no. 5, pp. 2140-2151, May 2008.

[9] T. Viitanen and H. Tussa, "The operation of the vector modulated and vector controlled Vienna I rectifier under distorted and unbalanced mains voltages," in *IEEE Proc. Appl. Power Electron. Conf. Expo.*, 2005, vol. 3, 2005, pp. 1680–1686.

[10] M. J. Newman, D. N. Zmood and D. G. Holmes, "Stationary frame harmonic reference generation for active filter systems," in *Proc. IEEE Appl. Power Electron. Conf. Expo.*, 2002, vol. 2, pp. 1054-1060.

[11] R. Burgos, R. Lai, Y. Pei, F. Wang, D. Boroyevich and J. Pou, "Space vector modulator for Vienna-type rectifiers based on the equivalence between two- and three-level converters: a carrier-based implementation," IEEE Trans. Power Electron., vol. 23, no. 4, pp. 1888-1898, July 2008.